

---

## Hydrothermal garnet in porphyry copper related skarn deposits, Ali-Abad, Yazd Province, Iran

B. Taghipour<sup>1\*</sup>, F. Moore<sup>2</sup>, M. A. Mackizadeh<sup>3</sup> and S. Taghipour<sup>4</sup>

<sup>1</sup>*Department of Earth Sciences, Faculty of Sciences, Shiraz University, Shiraz, Iran*

<sup>2</sup>*Department of Earth Sciences, Faculty of Sciences, Shiraz University, Shiraz, Iran*

<sup>3</sup>*Department of Geology, Faculty of Sciences, University of Isfahan, Isfahan, Iran*

<sup>4</sup>*Department of Geology, Faculty of Sciences, Tehran University, Tehran, Iran*

*E-mail: taghipour@shirazu.ac.ir*

---

### Abstract

The Ali-Abad porphyry copper deposit is located in the Central Iranian magmatic belt. As a result of subduction magmatism, Oligo-Miocene leucogranitoid rocks have intruded into conglomerates of lower Cretaceous age. Due to contact metamorphism the following mineral assemblage has occurred in the altered conglomerate: Garnet (andradite-grossular) + epidote + quartz + calcite + pyrite. Skarnification has only occurred in reactive carbonate clasts of the conglomerates. Chemical composition of garnets and classic discrimination scheme imply the porphyry copper related skarn-type mineralization. Garnets are characterized by abrupt chemical zoning and thin bands. REE pattern of skarn garnet and host granite have similar trends, so it is concluded that garnets are hydrothermal in origin. The garnet mineralization episode occurred during skarnification, giving hydrothermal fluid temperatures of 422-472 °C, likely this episode corresponds to the fluid boiling and high  $fO_2$  of garnet forming processes in the skarn system. Probably, the temporal decrease of hydrothermal fluid pressure led to rapid growths of andradite zones i.e., extensive hydrofracturing, porosity of conglomerate could be the dominant conditions which led to boiling of hydrothermal fluids and precipitation of andradite garnet.

**Keywords:** Garnet; skarn; copper deposit; hydrothermal fluids

---

### 1. Introduction

The Ali-Abad porphyry copper deposit is located 60 Km southeast of the city of Yazd in Taft-Yazd Province in central Iran. There is evidence of some ancient excavation workings by turquoise miners in the area. Geological work carried out by the French company COFIMINS resulted in the discovery of the porphyry copper deposits in 1972 [1].

The study area is located in the Cenozoic Magmatic Belt of Central Iran [2-4]. The belt is also known as the Uromieh-Dokhtar or Sahand-Bazman Belt, which forms a major porphyry copper province (Fig. 1). There are many skarn deposits which are associated with the plutons in the belt [5-15]. Due to its scientific and economic importance the area has been a subject of copper exploration activities and there are a number of published studies [16- 23].

The current study focuses on the detailed chemical zonation in garnets of the Ali-Abad skarns. The objective is to contribute to the overall understanding of the mineralogy, geochemistry and

genesis of the Ali-Abad skarn and, in particular, to provide information on the temporal variability of the hydrothermal system in which the skarns have been developed [24, 25].

### 2. Methodology

A total of fifty samples were collected for this study (Fig. 2). Twenty samples of monomineral garnet were separated by hand picking from crushed rock under a binocular microscope. The garnet separates were then powdered and leached in 10% hydrochloric acid (HCl) to dissolve carbonate minerals. The prepared samples were analyzed for REE and trace elements using Neutron Activation Analysis (NAA) at MNSR laboratory, Isfahan. Samples of intrusive rocks were analyzed for trace elements by Inductively Coupled Plasma Mass Spectrometry (ICP-MS) at Amdel Ltd. in Australia. International Standards AMH-1 and OU-3 were used as a quality control. Eight samples of Ali-Abad intrusive rocks were analyzed for major elements by XRF. Mineralogical composition of the garnets was determined using a Cameca SX50 electron microprobe at the University of Oklahoma, Norman (USA). Analytical condition for sulphates

---

\*Corresponding author

Received: 5 June 2012 / Accepted: 17 November 2012

was 20 kV accelerating voltage, 10 nA beam current and 20 μm defocused spot size. All elements were counted for 30 s on peak except for Fe (45 s), Mn (45 s) and Sr (60 s). This method yielded minimum detection levels in the 0.02-0.05 wt% oxide range for all components except for Ba (0.08 wt% BaO), Sr (0.08 wt% SrO) and S (0.08 wt% SO<sub>3</sub>) which are calculated at 3-sigma above mean background.

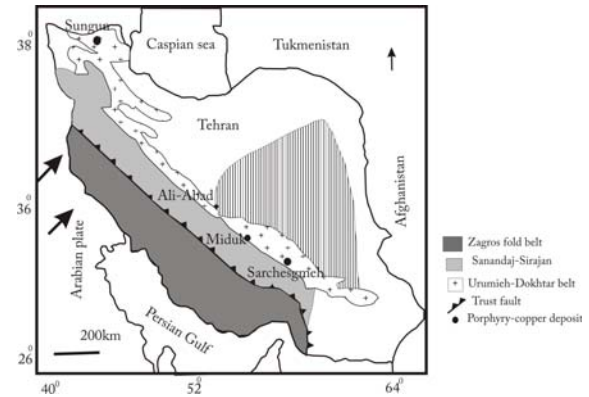


Fig. 1. Geological position of major porphyry copper deposits in relation to tectonic zones in Iran [26].

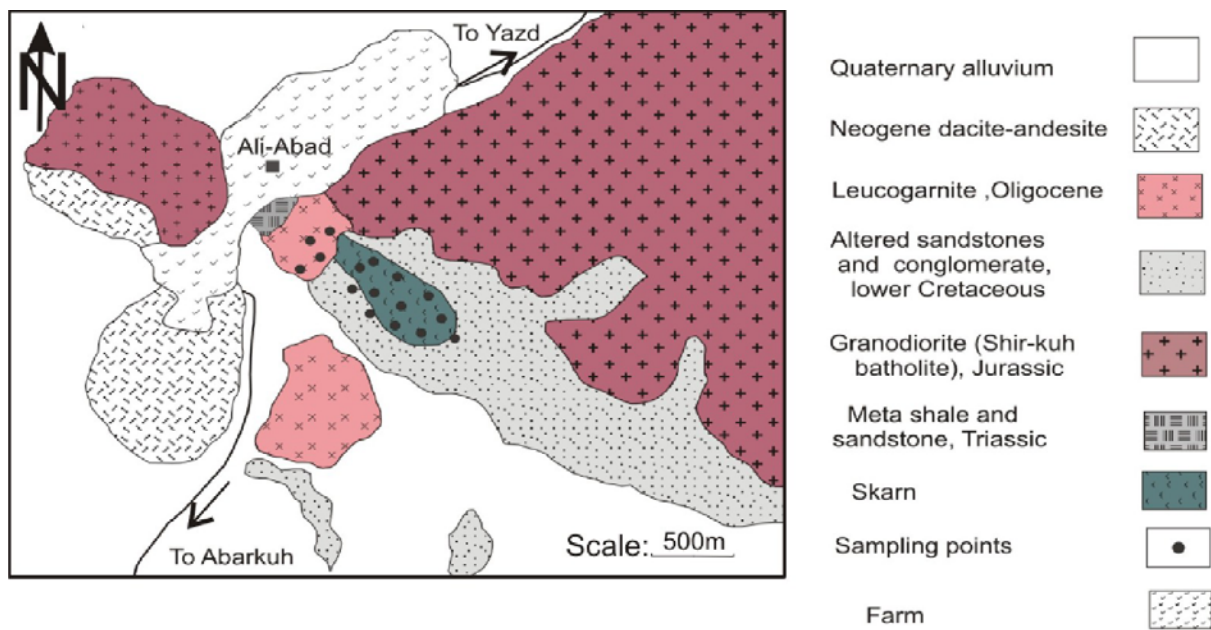
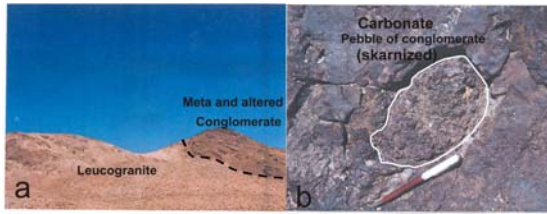


Fig. 2. Geological map of the Ali-Abad porphyry copper deposit showing sample sites location

### 3. Geological setting

The Ali-Abad porphyry copper deposit is located in the western margin of the Central Iranian Block within Cenozoic Magmatic Belt of Central Iran (Fig. 1). The oldest rock units in the area are the Middle Jurassic Shir-Kuh granitic batholith which intruded sedimentary rocks of Paleozoic and Triassic age [27, 2]. The batholith is unconformably overlain by lower Cretaceous conglomerate and sandstone units of the Sangestan Formation [27, 28, 19]. The conglomerate unit which is subject to hydrothermal alteration and skarn mineralization is composed of pebbles of different lithology (polymictic) and origin (polygenic). These rocks are overlain by conglomerate and volcano-sedimentary rocks of Eocene age. The volcanics consist mainly of andesitic lava related pyroclastic

rocks and dacitic domes. Oligo-Miocene granitoid stocks represent the youngest magmatic event in the Ali-Abad porphyry deposit [29, 20] (Fig 2). They consist of leucogranite, granite, granodiorite, diorite to gabbro in composition [30, 23]. These late intrusions also host the porphyry copper mineralization at Ali-Abad (Fig. 3a) [16]. Zarasvandi et al. [20], based on a pilot K/Ar dating study determined that the pre-mineralization granites were emplaced during the Oligocene.



**Fig. 3.** a. The pluton-host rock contact exposed at Ali-Abad. b. A large pebble of conglomerate which has been wholly replaced by a garnet bearing mineral assemblage. Other non-carbonaceous pebbles are unaltered.

Hydrothermal alteration of the intrusive rocks at Ali-Abad consists of propylitic, phyllic, argillic and advanced argillic alteration [31]. Quartz, sericite, muscovite, pyrite, epidote, chlorite, kaolinite, jarosite, turquoise and occasionally alunite represent the main alteration mineral assemblage. Phyllic alteration is the dominant alteration type and affects approximately 80 % of granite porphyry [30].  $^{40}\text{Ar}/^{39}\text{Ar}$  dates on secondary biotite and sericite indicate an alteration event took place in 16 years ago [20].

During the hydrothermal alteration of intrusive rocks, the conglomerate unit of the Snagestan Formation was also altered and skarn development occurred in limestone cements and fragments (pebbles and cobbles, Fig. 3b) of conglomerate. The main minerals in metamorphosed parts of the conglomerate are garnet, quartz, pyrite, and Fe oxides [28].

#### 4. Petrology of the Ali-Abad intrusion

The Ali-Abad intrusives consist mainly of hololeucocratic granite to granodiorite. The main mineralogical components are quartz, k-feldspar, Na-plagioclase, muscovite and rarely chloritized mafic minerals [22]. Micrographic intergrowths of quartz and alkali-feldspars and chessboard texture are common. There is evidence of high pressure, shattering texture (Fig. 4a) in Ali-Abad rocks probably due to hydrothermal hydrostatic pressures. Porphyritic (Fig. 4b) and granophyric (Fig. 4d) textures suggest a subvolcanic or hypabyssal nature for the intrusive body. Hydrothermal alteration mainly consists of quartz (silicification) development together with sericitization of biotite and alkali feldspars (Fig. 4c & 4e) and kaolinitization of feldspars (Fig. 4f).

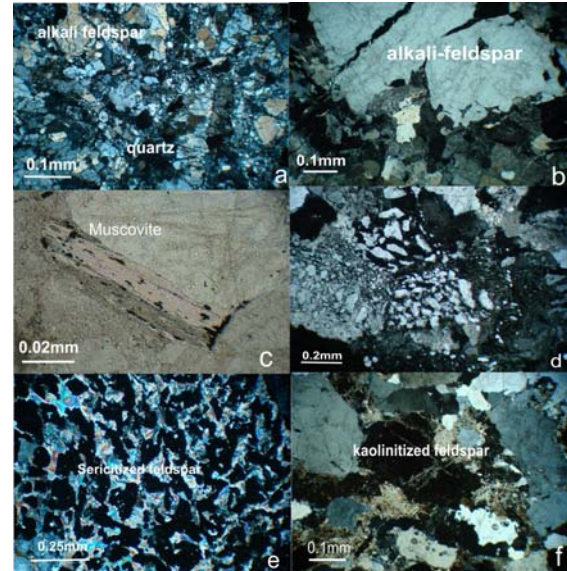


**Fig. 4.** a. Brecciated texture of felsic minerals. b. Porphyroid texture which developed from the existence of phenocrysts of anhedral quartz in the groundmass. c. Replacement of biotite crystal by muscovite. Opaque minerals, mainly magnetite, are aligned along cleavages. d. Granophyric intergrowth of quartz in the groundmass of alkali feldspar. e. Wholly sericitized feldspar, the dark parts are quartz which is extinct under crossed plars (XPL) isotropy. f. Kaolinitized rock, only the quartz crystals are preserved. The dark parts are kaolinitized alkali-feldspar.

Chemical analyses of Ali-Abad intrusion body (Table 1) shows that the rocks are in the compositional range of granite (mainly) to granodiorite (Fig. 5a) and are calc-alkaline character in magmatic series (Fig. 5b). Notably the molar ratio of  $\text{Al}_2\text{O}_3$  is higher than that of the  $\text{Na}_2\text{O} + \text{K}_2\text{O} + \text{CaO}$  molar ratios, so the intrusive rocks are peraluminous in nature (Fig. 5c).

Eslamzadeh [16] shows that these granites are I-type and believe they are differentiated felsic granitoid which resulted from partial melting of infracrustal region. Zarasvandi *et al.* [20] note that the intrusives at Ali-Abad show moderate to strong negative Eu anomalies and shallow-sloping MREE-HREE patterns in granitic rocks and LREE-enrichment and absence of negative Eu anomalies in quartz monzodioritic rocks. Trace element data from the current study indicates that a subduction related magmatism took place, because all samples are in the fields of volcanic arc and syncollision granites (Fig 5d and 5e). This is in agreement with Zarasvandi, *et al.* [20] who also concluded that the intrusives derived from I-type calc-alkaline arc-type magmas.

**Table 1.** Major and trace elements from samples of the Ali-Abad intrusive body

| Sample                           | DM-1   | DM-2  | DM-3  | DM-4  | DM-5  | DM-6  | DM-7  | DM-8  |
|----------------------------------|--------|-------|-------|-------|-------|-------|-------|-------|
| SiO <sub>2</sub> %               | 75.97  | 74.1  | 79.25 | 77.95 | 80.24 | 79.05 | 80.40 | 78.17 |
| Al <sub>2</sub> O <sub>3</sub> % | 14.23  | 14.7  | 12.54 | 12.78 | 11.97 | 12.47 | 11.87 | 13.49 |
| TiO <sub>2</sub> %               | 0.13   | 0.28  | 0.03  | 0.10  | 0.07  | 0.04  | 0.06  | 0.07  |
| FeO %                            | -      | -     | 0.62  | 0.53  | 0.58  | 0.47  | 0.45  | 0.45  |
| Fe <sub>2</sub> O <sub>3</sub> % | 1.07   | 1.00  | 0.03  | 0.11  | 0.06  | 0.09  | 0.03  | 0.00  |
| CaO %                            | 0.32   | 0.2   | 0.44  | 0.98  | 0.66  | 0.44  | 0.44  | 0.58  |
| MgO %                            | 0.2    | 0.21  | n.d   | 0.11  | n.d   | 0.04  | n.d   | 0.06  |
| K <sub>2</sub> O %               | 4.92   | 2.30  | 0.35  | 2.35  | 0.58  | 2.12  | 0.40  | 0.83  |
| Na <sub>2</sub> O %              | 3.27   | 6.72  | 6.54  | 4.86  | 5.43  | 4.79  | 6.01  | 5.71  |
| Y (ppm)                          | 36     | 8     | 10    | 9     | 21    | 25    | 4     | 10    |
| Nb (ppm)                         | 9      | 24    | 8     | 6     | 7     | 14    | 10    | 9     |
| Rb (ppm)                         | 200    | 51    | 74    | 71    | 33    | 12    | 4     | 43    |
| Total                            | 100.12 | 99.51 | 99.81 | 99.77 | 99.59 | 99.51 | 99.66 | 99.36 |

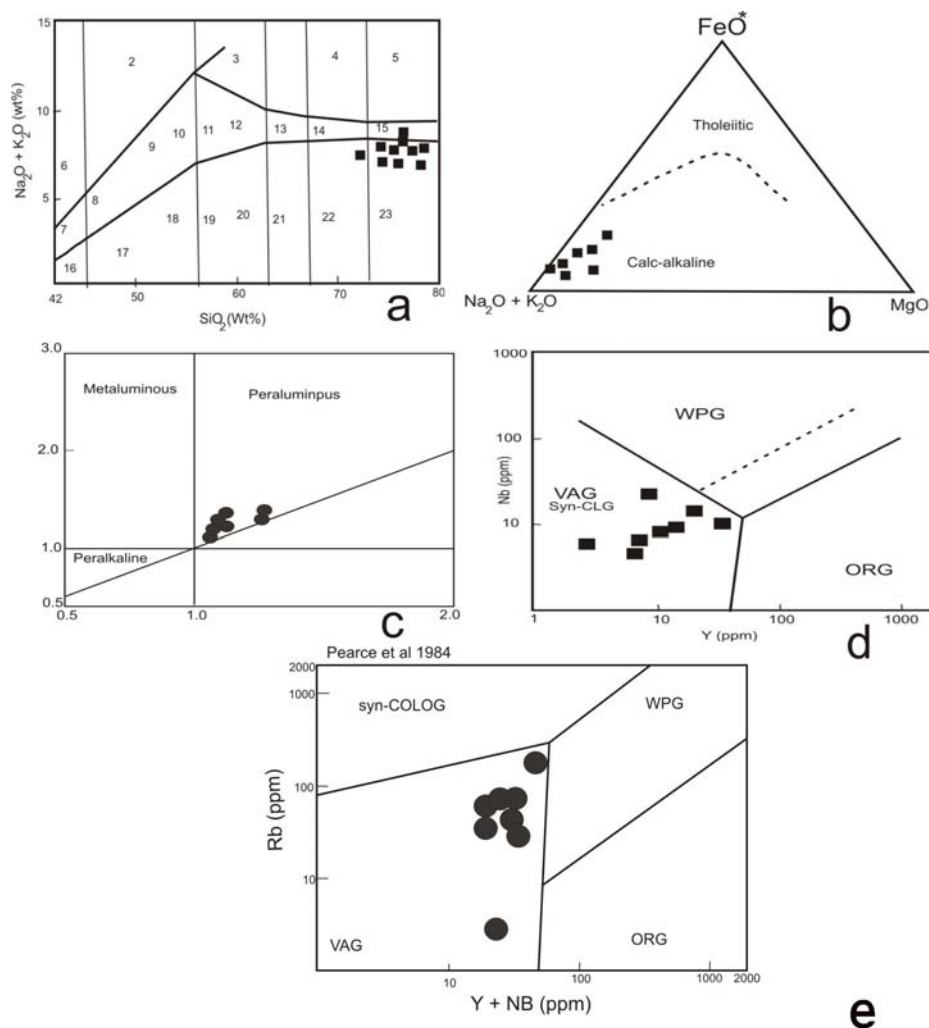


**Fig. 5.** a. Classification diagram of Middlemost [32] Ali-Abad data plots mainly in the fields of granite. b. AFM diagram and the position of Ali-Abad intrusion rocks in the calc-alkaline field [33]. c. Molar ratios of A/CNK versus A/NK. Ali-Abad granitoids showing peraluminous character [34]. d & e. Tectonic setting trace element discrimination diagrams for syn-collision (syn-colog), volcanic arc (VA), within-plate (WP), and ocean-ridge (OR) granites. Pearce et al's [35] diagram indicates the position of Ali-Abad stock within magmatic arc setting.

## 5. Skarn Mineralogy

As noted above, skarn development is restricted to the limestone pebbles and cements within the conglomerate unit. In some cases the entire carbonate pebbles may be replaced by skarn minerals. The predominant mineral assemblage observed in Ali-Abad skarn is:

Garnet + quartz + calcite + pyrite + epidote ± iron oxides

Garnet in hand specimen is chocolate brown to russet in color. In field outcrops garnet has sometimes been observed in calcite-quartz bearing geode like structures. Euhedral garnet crystal is also visible as open space filling. Euhedral and cube shaped oxidized pyrite crystals and clear quartz clusters are also common. In thin polish sections, porphyroblastic texture of garnet in calcite and quartz groundmass is common. In plain polarized light (PPL) garnet color varies from honey yellow to slightly colourless.

Most of the garnet grains show atoll texture and have distinct resorbed margins (Fig. 6a, b). As a result of oxidation or replacement some iron oxides were formed in the margin or within garnet grains (Fig. 6c). The garnets show some alteration and a number of grains were observed where garnet has been pseudomorphed by chlorite, calcite, quartz and iron oxides (Fig. 6d). Under crossed nicols (XPL) isotropy and anisotropy are both visible in garnet grains. In some cases the anisotropic margin of garnets is also visible in PPL with honey yellow color (PPL), the parts with complex zoning and twinning are prominent and overgrowth on colorless isotropic interiors (Fig. 6e and 6f). Another outstanding feature of skarn development is silicification which consists of late quartz replacement of carbonate groundmass and formation of microgranular quartz. Inclusions of a dispersed primary skarn classificate (tremolite-actinolite) and epidote which are often wholly replaced by calcite are also visible in quartz. Silicification is the latest phase of alteration and has affected all previous mineral assemblages.

## 6. Trace and REE geochemistry

REE patterns in granitoid complexes hosting Cu-porphyry mineralization are valuable tools in the elucidation of magma sources [36, 37]. Trace and REE elements analysis data (Table 2) of the intrusive rocks and garnet skarn from Ali-Abad have been normalized to primitive mantle (e.g. [38]).

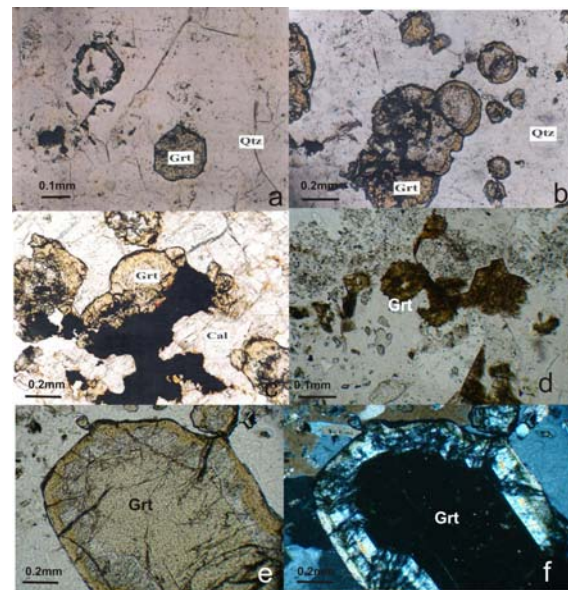


**Fig. 6.** a. Atoll texture, resorbed margin and relic of garnet showing later decomposition of garnet grains during quartz replacement. b. Garnet grains showing resorbed margins in a groundmass of quartz. There is a distinct overgrowth of honey yellow and an anisotropic rim on the inner colourless parts of the grain. c. Replacement of iron oxide within garnet and granular calcite in the groundmass. d. Replacement of garnet grains by chlorite. e & f. Complex zoning and twinning in coarse garnet

The REE pattern of the studied intrusive rocks, in general, displays slightly LREE enrichment and HREE depletion (Fig. 7a) and a negative Eu anomaly similar to that reported by Zarasvandi *et al.* [19, 20]. Negative Eu anomalies ( $\text{Eu}/\text{Eu}^* = 0.01-0.53$ ) is suggestive for plagioclase fractionation during differentiation of the magma. LREE-enrichment combined with the lack of an Eu negative anomaly ( $\text{Eu}/\text{Eu}^* = 0.01-0.53$ ) and  $(\text{La}/\text{Yb})_n$  average values = 158.21 indicate that hornblende fractionation controlled differentiation of quartz monzodiorite–granodiorite parent magmas [1, 20]. The trace element pattern (Fig 7b) displays positive anomalies in Rb, Th, Ba and K and negative anomalies for Nb, which is characteristic of arc magmas [39].

The REE analysis patterns for garnet samples which are normalized to shale composite NA. Fig. 7c distinctly indicates of LREE depletion and HREE enrichment. This is characteristic for andradite type garnets which have been evolved in high  $f\text{O}_2$ . Also, high oxidation state of their geologic environment is reflected by Eu negative anomaly. Furthermore, the Eu depletion pattern indicates that Eu was differentiated as  $\text{Eu}^{3+}$  during high  $f\text{O}_2$  of fluids [40, 41]. The degree of Eu depletion in garnet correlates with that of the

intrusive rocks [40]. Also, other trace element patterns for garnet are similar to those of the intrusive rocks (Fig. 7d). Finally, the similar behavior of Eu in the intrusive and garnet related

skarn may be indicative of the same physicochemical condition of hydrothermal skarn forming fluids.

**Table 2.** ICP\_MS data of trace and REE elements from Ali-Abad intrusive rocks

| Element /ppm | D-1   | D-2   | D-3   | D-4   | D-5    | D-6   | D-7    | D-8    |
|--------------|-------|-------|-------|-------|--------|-------|--------|--------|
| La           | 15    | 13    | 18    | 34    | 31     | 37    | 20     | 28     |
| Ce           | 20    | 14    | 20    | 25    | 28     | 18    | 32     | 30     |
| Pb           | 13.5  | 36.5  | 17.5  | 21    | 90.50  | 48    | 48     | 99.5   |
| Pr           | 3.42  | 4.40  | 5.6   | 6.51  | 5.90   | 5.10  | 4.70   | 3.20   |
| Mo           | 25.5  | 17.5  | 20    | 27    | 7.80   | 50.75 | 75     | 11     |
| Sr           | 63.5  | 621   | 78    | 311.5 | 16.20  | 29    | 23     | 24     |
| Nd           | 11    | 7.10  | 13    | 30    | 2.30   | 1.20  | 2.18   | 2.43   |
| Sm           | 2.10  | 1.30  | 1.42  | 1.53  | 102    | 124   | 109    | 111.5  |
| Zr           | 139.5 | 85.5  | 122.5 | 98    | 1.40   | 1.21  | 1.70   | 0.68   |
| Eu           | 0.74  | 0.61  | 0.57  | 1.60  | 1.48   | 1.40  | 1.80   | 1.55   |
| Gd           | 1.00  | 0.76  | 0.98  | 1.50  | 0.48   | 0.32  | 0.18   | 0.20   |
| Tb           | 0.16  | 0.23  | 0.7   | 0.16  | 1.02   | 0.54  | 0.98   | 0.89   |
| Dy           | 0.89  | 0.67  | 0.90  | 0.65  | 25     | 15.5  | 27     | 19.5   |
| Y            | 0.29  | 21    | 19    | 18.5  | 0.36   | 0.27  | 0.38   | 0.51   |
| Ho           | 0.20  | 0.17  | 0.56  | 0.47  | 0.67   | 0.98  | 0.17   | 0.46   |
| Er           | 0.54  | 0.32  | 0.51  | 0.48  | 0.04   | 0.19  | 0.00   | 0.02   |
| Tm           | 0.04  | 0.03  | 0.01  | 0.00  | 1.30   | 0.57  | 0.43   | 0.18   |
| Yb           | 0.51  | 0.45  | 0.30  | 0.98  | 0.14   | 0.08  | 0.12   | 0.12   |
| Lu           | 0.03  | 0.05  | 0.19  | 0.08  | 34.5   | 56.5  | 23     | 29.5   |
| V            | 32.5  | 34.5  | 33.5  | 31    | 1.00   | 12    | 31.5   | 126.5  |
| Cr           | 147.5 | 103.5 | 135.5 | 99.5  | 7.50   | 9.50  | 15.5   | 9.00   |
| Ni           | 7.00  | 11.5  | 6.50  | 7.50  | 2.50   | 11.75 | 39.5   | 682.5  |
| Cu           | 140   | 314.5 | 918.5 | 5.20  | 93     | 166.5 | 25     | 333.5  |
| Zn           | 25    | 119.5 | 59.5  | 125.5 | 13     | 732.5 | 66     | -      |
| Eu/Eu*       | 0.23  | 0.29  | 0.24  | 0.53  | 0.01   | 0.01  | 0.01   | 0.01   |
| La/Lu        | 29.41 | 58    | 60    | 34.69 | 221.42 | 462.5 | 166.66 | 233.33 |

**Table 3.** NAA analyses of trace and REE elements of Ali-Abad garnet separates

| Sample No. | S.DM8 | S.DM6 | S.DM7 | S.DMZ |
|------------|-------|-------|-------|-------|
| Ag         | 3     | 2     | 4     | 3     |
| Au         | 18    | 14    | 15    | 15    |
| Hg         | 1.10  | 1.12  | 1.03  | 1.12  |
| Rb         | 20    | 10    | 11    | 12    |
| Cs         | 1.3   | 1.50  | 1.42  | 1.62  |
| Ga         | 11    | 10    | 10.21 | 11.30 |
| Ta         | 0.70  | 0.60  | 0.70  | 0.70  |
| Hf         | 0.7   | 0.4   | 1.20  | 0.8   |
| Th         | 0.35  | 0.31  | 0.54  | 0.37  |
| U          | 1.10  | 1.12  | 1.63  | 1.21  |
| La         | 3.40  | 3.42  | 3.21  | 3.46  |
| Ce         | 12.40 | 12.41 | 13.25 | 12.36 |
| Nd         | 27.18 | 91.2  | 31.45 | 27.98 |
| Sm         | 1.39  | 12.5  | 10.54 | 11.41 |
| Eu         | 0.31  | 3.21  | 2.20  | 3.12  |
| Gd         | 0.28  | 1.65  | 1.23  | 1.43  |
| Tb         | 0.22  | 0.21  | 0.21  | 0.23  |
| Dy         | 1.40  | 1.35  | 1.23  | 1.43  |
| Ho         | 0.36  | 0.56  | 0.51  | 0.52  |
| Tm         | 0.12  | 0.42  | 0.14  | 0.17  |
| Yb         | 0.45  | 0.98  | 0.89  | 0.91  |
| Lu         | 0.50  | 0.64  | 0.54  | 0.54  |
| Eu/Eu*     | 0.37  | 0.45  | 0.37  | 0.48  |
| La/Lu      | 6.80  | 5.34  | 5.94  | 6.40  |

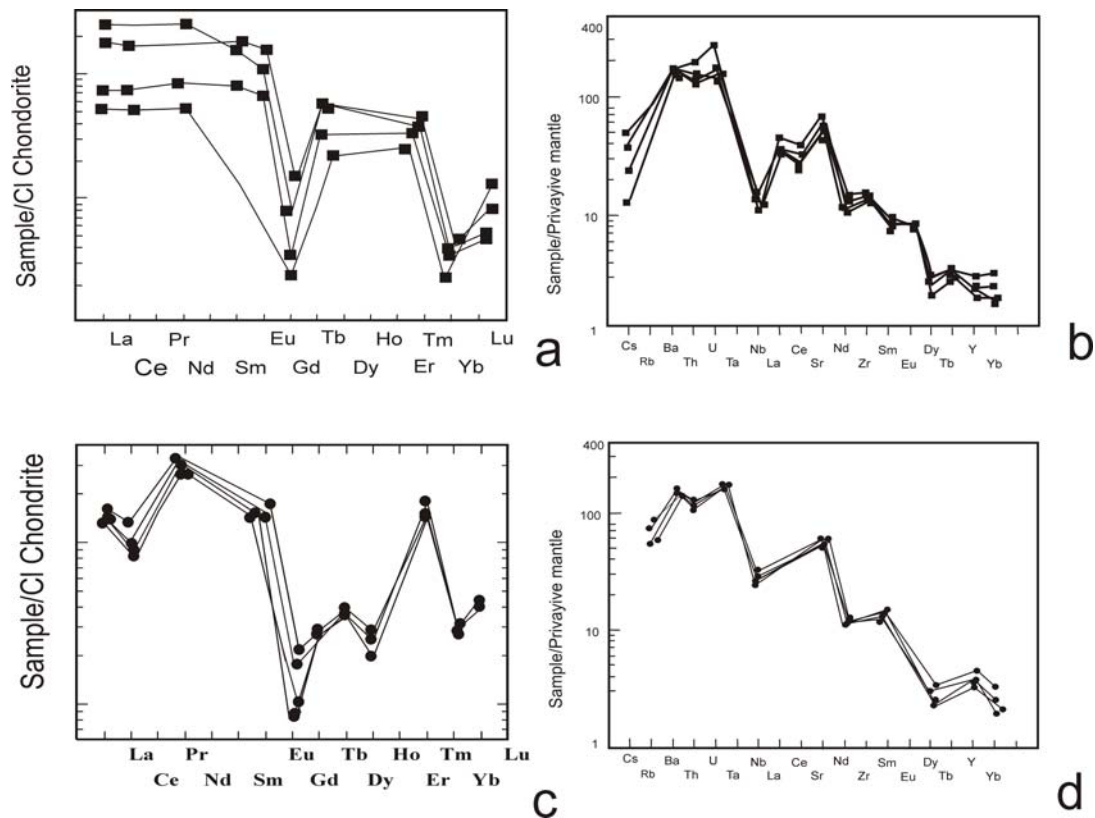


Fig. 7. a, b. REE and trace element patterns for Ali-Abad intrusive rocks.  
c & d. REE and trace element patterns of garnet separates

## 7. Garnet mineralogy

As noted above, garnets from Ali-Abad skarn are characterized by optically complex growth zoning under the microscope. For better recognition of these micro structures back scattered electron (BSE) micrograph images were also studied. Garnet from skarn analyzed with the electron microprobe (Table 4) shows abrupt zoning parts or bands (Fig. 8a and 8b). The chemical composition of these zones implies that garnet grains are compositionally inhomogeneous. There is an obvious abrupt

chemical compositional change across oscillatory zones. It is concluded that this is caused by an increase in the andradite over grossular component of garnet in solid solution. Some of these zones have sharp margins (Fig. 8a) whereas others show corrosional margin (Fig. 8b) indicating unstable boundaries. The latter feature may have resulted from reaction of an existing zone in the mineral grain with younger hydrothermal fluids under different conditions.

Table 4. Representative electron microprobe analyses of garnet

| Label         | No | SiO <sub>2</sub> | TiO <sub>2</sub> | Al <sub>2</sub> O <sub>3</sub> | FeO   | MnO  | MgO  | CaO   | Total |
|---------------|----|------------------|------------------|--------------------------------|-------|------|------|-------|-------|
| DM2-1         | 5  | 37.20            | 0.10             | 13.41                          | 12.32 | 0.69 | 0.00 | 35.20 | 98.92 |
| DM2-1         | 6  | 36.77            | 0.00             | 11.97                          | 13.81 | 0.71 | 0.00 | 34.88 | 98.14 |
| DM2-2rim      | 7  | 36.63            | 0.03             | 11.48                          | 14.61 | 0.72 | 0.00 | 34.80 | 98.27 |
| DM2-G1inter-1 | 8  | 35.27            | 0.00             | 0.06                           | 28.18 | 0.23 | 0.02 | 33.08 | 96.84 |
| DM2-G1inter-2 | 9  | 35.16            | 0.02             | 0.06                           | 28.09 | 0.23 | 0.01 | 33.33 | 96.91 |
| DM2-G1rim-1   | 10 | 35.00            | 0.03             | 0.04                           | 28.86 | 2.33 | 0.01 | 30.90 | 97.15 |
| DM2-G1rim-2   | 11 | 34.03            | 0.04             | 0.06                           | 28.88 | 2.47 | 0.00 | 30.78 | 96.25 |

**Table 4.** (Continued)

|                  |    |       |      |       |       |      |      |       |       |
|------------------|----|-------|------|-------|-------|------|------|-------|-------|
| DM2-G2-core-1    | 12 | 35.54 | 0.02 | 0.10  | 28.26 | 0.31 | 0.10 | 33.07 | 97.40 |
| DM2-G2-core-2    | 13 | 35.36 | 0.00 | 0.03  | 28.44 | 0.28 | 0.13 | 32.99 | 97.23 |
| DM2-G2-interio-1 | 14 | 34.98 | 0.00 | 0.08  | 28.75 | 2.59 | 0.00 | 29.96 | 96.36 |
| DM2-G2-rim-1     | 15 | 36.76 | 0.66 | 6.97  | 20.90 | 1.87 | 0.01 | 32.01 | 99.16 |
| DM2-G2-rim-2     | 16 | 36.76 | 0.32 | 7.05  | 20.99 | 1.67 | 0.00 | 32.10 | 98.89 |
| DM2-G2-inc-1     | 17 | 36.54 | 0.47 | 6.92  | 20.05 | 1.23 | 0.00 | 33.43 | 98.65 |
| DM2-G2-inc-2     | 18 | 37.25 | 0.23 | 8.44  | 17.82 | 0.49 | 0.04 | 34.74 | 99.02 |
| DM3-Ep4-dark     | 22 | 37.63 | 0.09 | 24.32 | 11.43 | 0.12 | 0.00 | 23.52 | 97.11 |
| DM3-Ep4-brite    | 23 | 37.34 | 0.06 | 21.60 | 14.85 | 0.13 | 0.00 | 23.14 | 97.11 |
| DM3-G1-core      | 24 | 34.96 | 0.00 | 0.29  | 27.97 | 0.55 | 0.02 | 32.92 | 96.71 |
| DM3-G1-core2     | 25 | 33.63 | 0.01 | 0.01  | 28.18 | 0.45 | 0.03 | 32.85 | 95.16 |
| DM3-G1-intrim-1  | 26 | 36.86 | 0.12 | 9.71  | 16.57 | 0.71 | 0.03 | 34.52 | 98.53 |
| DM3-G1-extrim-1  | 27 | 36.82 | 1.15 | 9.35  | 17.28 | 3.97 | 0.00 | 30.27 | 98.83 |
| DM3-G2-core1     | 28 | 35.74 | 0.04 | 0.06  | 28.21 | 0.46 | 0.03 | 32.83 | 97.36 |
| DM3-G2-core2     | 29 | 35.73 | 0.02 | 0.13  | 27.96 | 0.48 | 0.04 | 33.03 | 97.39 |
| DM3-G2-interior1 | 30 | 37.85 | 0.00 | 13.04 | 12.11 | 0.81 | 0.01 | 35.25 | 99.07 |
| DM3-G2-interior2 | 31 | 37.05 | 0.08 | 12.61 | 12.73 | 0.84 | 0.01 | 35.21 | 98.53 |
| DM3-G2-rim1      | 32 | 35.94 | 0.83 | 8.77  | 17.90 | 4.75 | 0.00 | 29.42 | 97.61 |
| DM3-G2-rim2      | 33 | 36.85 | 0.77 | 9.49  | 17.68 | 5.10 | 0.00 | 28.97 | 98.85 |

The compositional variations of the garnets in Ali-Abad skarn are graphically presented in Fig. 9 together with garnets from other mineralized skarns worldwide [42]. The compositions of Ali-Abad garnets are in the range of those from most well known Cu-Mo-Fe skarn deposits.

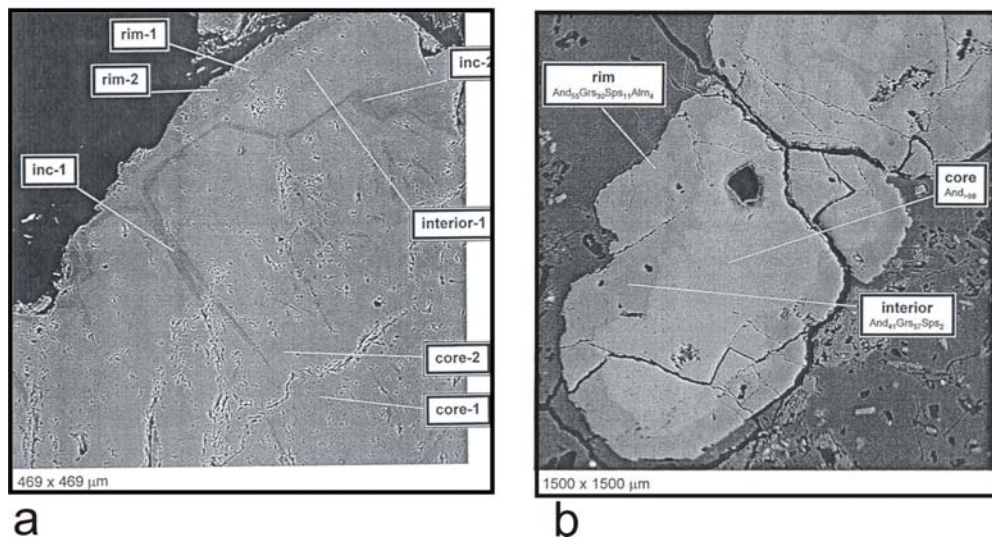


**Fig. 8.** a. BSE image of garnet showing zoning in quartz groundmass (dark part). b. Garnet grain showing zoning, corroded margins and abrupt changes in chemical composition from centre to margin

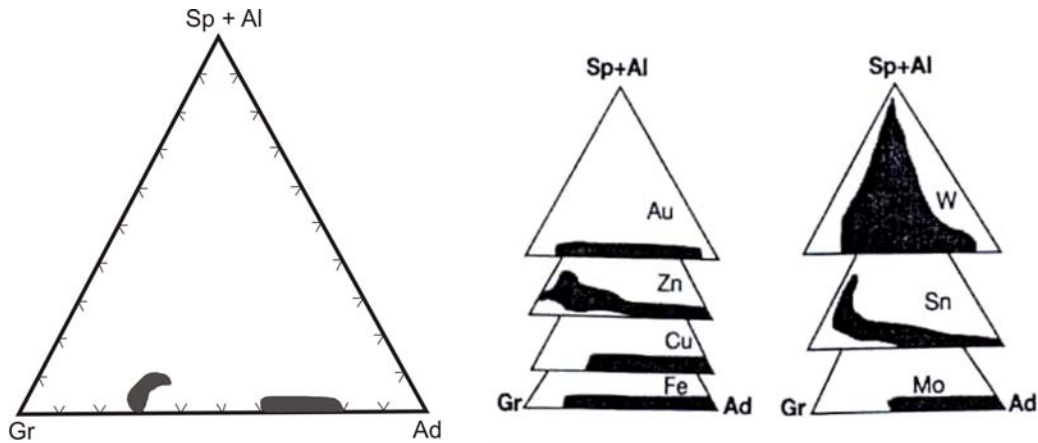


**Fig. 9.** Gr-Ad- (Al+ Sp) diagram is showing average chemical composition of Ali-Abad garnet (a) and according to the classic scheme of Meinert [51] (b)

Grossular-andradite garnets and their complex zoning are sensitive to changes in fluid composition and should therefore mirror the fluid evolution in skarn assemblage [25]. Thin or narrow compositional zones represent periods of slow growth rates between pulses of hydrothermal fluids. The zonation patterns visible in garnets from Ali-Abad skarns record at least intermittent growth periods. Subsequent rapid, epitaxial growth of andradite rich garnet on grossular-rich cores is interpreted to mark the onset of vigorous and focused fluid flow along high-permeability zones. As noted before, these zones have been developed by the existence of reactive, permeable pebbles in host conglomerates. All together the fluid flow canalization by the high permeability of the host conglomerate may be play a role in compositional changes of garnet, which is shown by complex zoning [43].

Fluid boiling is an important mechanism involved in the precipitation of minerals in hydrothermal systems. There is a large volume of literature dealing with the effect of fluid boiling on the hydrothermal systems and mineral precipitation [44, 25]. Boiling is possible as a consequence of tectonic pressure-reduction. Boiling could cause the temperature of the fluids to decrease, resulting in rapid escape of  $H_2S$  and  $CO_2$ , and concentration of solutes, leading to precipitation of quartz, carbonates and sulphides. Similar simple mineral assemblage could account for such a mechanism in the skarn garnet genesis in Ali-Abad and characterizes the principal stage of skarn development at the deposit [45-48]. Briefly, the hydrothermal fluids of the Ali-Abad skarn were derived essentially from magma source. Multi-episodes of boiling of these late-magmatic and post-magmatic fluids accelerated garnet forming processes (Fig. 10).

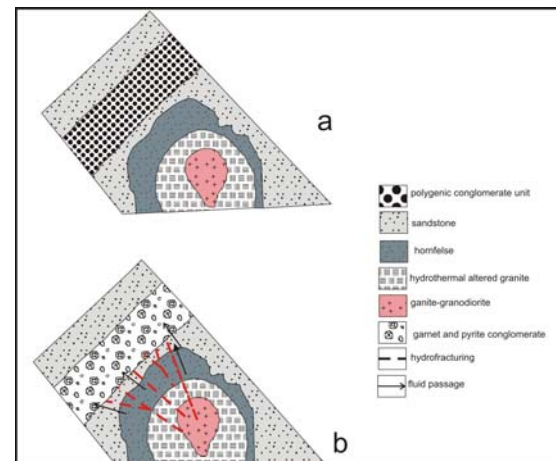


**Fig. 10.** Schematic model of skarn formation in permeable conglomerate unit at Ali-Abad. a. Intrusion, solidification and hydrothermal alteration of intrusion body. b. Increasing hydrothermal fluid pressure within intrusion leads to hydrofracturing and sudden release of fluids through veins, fractures toward permeable conglomerate

The intrusive body at Ali-Abad, similar to other Cu-porphyry intrusion bodies is from shallow level emplacement. Extensive fracturing and brecciation is confined to the intrusive body and surrounding rocks and there is no evidence of fracturing caused by regional tectonics. Therefore it is concluded that the fractures are formed by hydraulic fracturing [22]. In association with that, volume contraction during cooling phase of the intrusive body probably has played an important role on the reduction of fluid pressure. This resulted in open space from the above mentioned dynamic mechanisms in addition to conglomerate environment, which can give rise to exsolution of volatile components and an increase in the quantity of ascending bubbles in the hydrothermal fluids.

By using stable isotope data on garnet with oscillatory zoning [49] it has been concluded that, zones with high  $Fe^{+3}/Al$  show high  $\delta^{18}O$  values which are characteristic of magmatic fluids derived from intrusion body during the emplacement and crystallization. Zones with low  $Fe^{+3}/Al$  originated from meteoric fluids highlighted by lower  $\delta^{18}O$  values.

According to Gaspar *et al.* [41] Al – rich garnets formed by diffusive metasomatism, at low water/rock ratios, from host-rock buffered metasomatic fluids. Fe-rich garnets grow rapidly by advective metasomatism, at higher W/R ratios, from magmatic-derived fluids, consistent with an increase in porosity by fracturing.

Yardly *et al.* [50] describe that fluid flow in hydrothermal systems is always associated with boiling process, which follows oxidation of fluid, increasing in  $Fe^{+3}/Al^{+3}$  and finally rapid grow of andradite garnet. According to Jamtveit [25] removing pressure on the hydrothermal system and following hydrothermal boiling could result in high  $fO_2$  of fluids and growth andradite garnet.

## 8. Skarn formation conditions

The principal constituents of skarns at Ali-Abad are garnet, quartz and calcite, so it seems that the system Fe-Si-C-O-H [52] is most appropriate to determine the temperature-oxygen fugacity ( $T - fO_2$ ) stability field of the garnet as the main constituent of skarn. Fig. 11 shows a  $T - fO_2$  diagram which is based on 0.5 Kbar total pressure and  $XCO_2 = 0.1$  [i.e.  $CO_2 / (CO_2 + H_2O) = 0.1$ ]. There is evidence of some features regarding subvolcanic or hypabyssal nature of intrusion body like porphyroid, microgranular to aplitic texture to support this pressure, also large limestone pebbles constitute the conglomerate, accounting for the evaluation the  $XCO_2 = 0.1$  mineralization fluids.

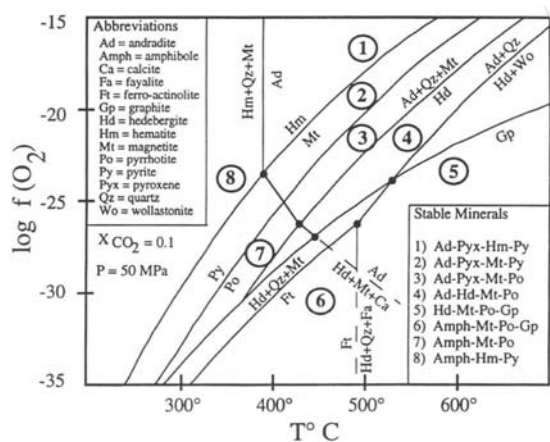


**Fig. 11.** Temperature –  $\log fO_2$  diagram at 500 bar and  $XCO_2=0.1$  for the system

## 9. Conclusions

1. The spatial relationship between the study skarn and the Ali-Abad porphyry copper stock indicates that skarn formation took place sharply, far from intrusion so the skarn can be classified as a distal type skarn. This is the first report of distal skarn in the Central Iran magmatic arc.
2. The process of growth of andradite garnet is related to depressurization of the hydrothermal system, which in turn resulted in boiling and increasing  $fO_2$  in the hydrothermal fluids which facilitated andradite deposition.
3. High ratio of water-rock interaction probably existed in the permeable zones which were also preferential for the hydrothermal solutions transportation. High permeability in the conglomeratic horizon provided open spaces or interstices for local and sudden reduction of lithostatic pressure during the introduction, invading, canalization and circulation of the hydrothermal fluids. Open space filling or geode forming structures of the hydrothermal minerals at Ali-Abad support this process.
4. Boiling and hydraulic fracturing played an important role in mineral deposition as evolved changes in fluid chemistry as a result of interaction with open spaces or zones of high permeability.
5. The strong hydro-fracturing associated with a shallow level intrusion greatly increases the channel ways for the hydrothermal fluids and hence filled out with fluids derived from magmatic source.
6. The good correlation between REE patterns of the intrusive rocks and garnets in related skarn indicate that the garnets were formed from hydrothermal fluids, derived from the same magmatic source. These fluids most likely moved via hydrofracturing channel ways.

In general the style processes of skarn development which are porphyry system related also depend on the hydrothermal processes involved in porphyry intrusion body.

## Acknowledgments

The authors are grateful to the research committee of Shiraz University, for supporting this project. We are very grateful to Dr. G. Fernette (USGS) and Dr. D. Marinov (SEG Mentor, Senior Geologist, Anglo American Perú) for their constructive comments and advice. We thank Dr. F. Daliran for her assistance in carrying out the EPMA analyses at Karlsruhe University.

## References

- [1] Zarasvandi, A., Liaghat, S. & Zentilli, M. (2004). Evolution of the Darreh-Zerreshk and Ali-Abad porphyry copper deposits, central Iran, within an orogen-parallel strike-slip system [abs.]: in *30th Annual Meeting of Atlantic Geoscience Society*, January 30-31, Canada, Moncton, New Brunswick.
- [2] Forster, H. (1978). Mesozoic-Cenozoic metallogenesis in Iran. *J Geological Society of London*, 135, 443-445.
- [3] Jankovic, S. (1977). The copper deposits and geotectonic setting of the Tethyan Eurasian metallogenic belt: *Mineral Deposita*, 12, 37-47.
- [4] Amidi, S. M., Emami, M. H. & Michel, R. (1984). Alkaline character of Eocene volcanism in the middle part of Iran and its geodynamic situation. *Geol Rundschau*, 73, 917-932.
- [5] Somarin, A. K. & Moayyed, M. (2002). Granite- and gabbroiorite-associated skarn deposits of NW Iran. *Ore Geology Review*, 20, 127-138.
- [6] Calagari, A. A. (2003). Stable isotope (S, O, H and C) studies of the phyllic and potassic-phyllic alteration zones of the porphyry copper deposit at Sungun, East Azarbaijan, Iran. *Journal of Asian Earth Science*, 21, 767-780.
- [7] Calagari, A. A. (2004). Fluid inclusion studies in quartz veinlets in the porphyry copper deposit at Sungun, East-Azarbaijan, Iran. *Journal of Asian Earth Science*, 23, 179-189.
- [8] Somarin, A. K. (2004). Garnet composition as an indicator of Cu mineralization: evidence from skarn deposits of NW Iran. *Journal of Geochemical Exploration*, 81, 47-57.
- [9] Somarin, A. K., Liaghat, S., Hosseini A. & Zarasvandi, M. (2005). *World Skarn Deposits: Iran*. Digital Appendix to Meinert L. D., Dipple, G., Nicolescu, S., 2005, *World Skarn Deposits*: in Hedenquist J. W. Thompson, J. F. H., Goldfarb, R. Richards, J. P. (eds.), *Economic Geology One Hundredth Anniversary Volume*, Society of Economic Geologists, Littleton, CO., 2 p.
- [10] Calagari, A. A. & Hosseinzadeh, G. (2006). The mineralogy of copper-bearing skarn to the east of the Sungun-Chay river, East-Azerbaijan, Iran. *Journal of Asian Earth Science*, 28, 423-438.
- [11] Hezarkhani, A. (2006a). Mineralogy and fluid inclusion investigations in the Reagan Porphyry System, Iran, the path to an uneconomic porphyry copper deposit. *Journal of Asian Earth Science*, 27, 598-612.
- [12] Hezarkhani, A. (2006b). Petrology of the intrusive rocks within the Sungun Porphyry Copper Deposit, Azerbaijan, Iran. *Journal of Asian Earth Science*, 27, 326-340.
- [13] Mollai, H., Sharma, R. & Pe-Piper, G. (2009). Copper mineralization around the Ahar batholith, north of Ahar (NW Iran). Evidence for fluid evolution and the origin of the skarn ore deposit. *Ore Geology Review*, 35, 401-414.
- [14] Hezarkhani, A. (2009). Hydrothermal fluid geochemistry at the Chah-Firuzeh porphyry copper deposit, Iran. Evidence from fluid inclusions. *Journal of Geochemical Exploration*, 101, 254-264.
- [15] Boomeri, M., Nakashima, K. & Lentz, D. R. (2009). The Miduk porphyry Cu deposit, Kerman, Iran: A geochemical analysis of the potassic Zone including halogen element systematics related to Cu mineralization processes. *Journal of Geochemical Exploration*, 103, 17-29.
- [16] Eslamzadeh, E. (2002). Petrology of igneous rocks of the Ali-Abad and Darreh Zereshk (Yazd province Central Iran) and related Cu mineralization: Unpublished PhD thesis, Islamic Azad University of Iran. *Sc. And Re. Unit*.
- [17] Zarasvandi, A., Liaghat, S. & Ghayouri, K. (2002a). Geochemical characteristics and tectonic setting of Darreh-Zerreshk and Ali-Abad, southwestern Yazd Province: in 21st Earth Sciences Symposium of Iran: Teheran, Iran, *Geological Survey of Iran* (in Farsi with English abstract) 481-482.
- [18] Rezaian, K., Noghreian, M., Mackizadeh, M. A. & Sherafat, S. (2003). Geology and genesis of turquoise mineral indice, Ali-Abad (Taft-Yazd). *Journal of Science University of Isfahan*, 18, 145-158.
- [19] Zarasvandi, A., Liaghat, S. & Zentill, M. (2005). Geology of the Darreh-Zereshk and Ali-Abad porphyry copper deposits, Central Iran. *Int Geol Rev*, 47, 620-646.
- [20] Zarasvandi, A., Liaghat, S., Zentilli, M. & Reynolds, P. H. (2007).  $^{40}\text{Ar}/^{39}\text{Ar}$  Geochronology of Alteration and Petrogenesis of Porphyry Copper-Related Granitoids in the Darreh-Zerreshk and Ali-Abad area, Central Iran. *Explor Min Geol*, 16, 11-24.
- [21] Asadollahi, P., Khalili, M. & Mackizadeh, M. A. (2006). Garnet genesis in altered conglomerate of Sangestan Formation, Ali-Abad Aliabad (West of Taft, Yazd province). *Iranian Journal of Crystallography and Mineralogy*, 2, 263-278.
- [22] Taghipour, B. (2007). Mineralogical and geochemical studies of the hydrothermal alteration in the Cenozoic magmatic belt, Central Iran (Isfahan Province), West Alborz, Tarom Zone (Ghazvin Province): Unpublished PhD thesis in Farsi (with English abstract), *Isfahan University*.
- [23] Mackizadeh, M. A. (2008). Mineralogical and petrological studies of Central Iranian skarns (Yazd Province). Unpublished PhD thesis, in Farsi (with English abstract), Shahid Beheshti University.
- [24] Stowell, H. H. & Menard, T. (1998). Chemical zonation of contact metamorphism garnet: A record of fluid-rock interaction: Juneau gold belt, SE Alaska: Proceedings of the 9<sup>th</sup> Int. Symp. on Water-rock Interaction, Aehart and Hulston (eds) Balkema. *Rotterdam*, 421-426.
- [25] Jamtveit, B., Wogelius, R. A. & Fraser, D. G. (1993). Zonation pattern of skarn garnets: Records of hydrothermal system evolution. *Geology*, 21, 113-116.
- [26] Sokoutis, D., Bonini, M., Medvedev, S., Boccaletti, M., Talbot, C. J. & Oyi, H. (2000). Indentation of a continent with a built-in thickness change: Experiment and nature. *Tectonophysics*, 320, 243-270.
- [27] Nabavi, M. H. (1972). Geologic map of Yazd quadrangle, scale 1:250,000. *Geological Survey of Iran*, Tehran, Iran.
- [28] Khosrotehrani, K. & Vazirimoghadam, H. (1993). Stratigraphy of Lower Cretaceous in south and

- southwest of Yazd. *Journal of Earth Science*, 7, 43-57 (in Farsi).
- [29] Zarasvandi, A., Liaghat, S. & Carranza, E. J. M. (2002b). Petrology of igneous rocks of the Ali Abad and Darreh Zereshk (Yazd Province, Central Iran) and related Cu mineralization: Unpublished PhD thesis, Islamic Azad University of Iran.
- [30] Taghipour, B. & Noorbehesht, I. (2007). The occurrences of turquoise in advanced argillic alteration of Darreh-Zereshk and Ali-Abad porphyry copper deposits, Taft-Yazd Province, Central Iran. *Goldschmidt Conference Abstracts*, A9992.
- [31] Mackizadeh, M. A. & Taghipour, B. (2010). Mineralogical and geochemical studies of North West of Yazd skarn. *Geophysical Research Abstracts*, 12, 1633.
- [32] Middlemost, E. A. K. (1989). Iron oxidation ratios, norms and the classification of volcanic rocks. *Chemical Geology*, 77, 19-26.
- [33] Irvine, T. N. & Baragar, W. K. A. (1971). A guide to the chemical classification of the common volcanic rocks. *Canadian Journal of Earth Sciences*, 8, 523-548.
- [34] Maniar, P. D. & Piccoli, P. M. (1989). Tectonic discrimination of granitoids. *Geological Society of America*, 101, 635-643.
- [35] Pearce, J. A., Harris, N. B. W. & Tindle, A. G. (1984). Trace element discrimination diagrams for the tectonic interpretation of granitic rocks. *Journal of Petrology*, 25, 956-983.
- [36] Hanson, G. N. (1980). Rare earth elements in petrogenetic studies of igneous system. *Annual Review Earth Planetary Science*, 8, 371-406.
- [37] Nicolas, I. A. & Harrison, K. L. (1980). Experimental rare earth element partition coefficients for garnet, clinopyroxene and amphibole coexisting with andesite and basalt liquids: *Geochemica et Cosmochemica Acta*, 44, 287-368.
- [38] Sun, S. & McDonough, W. F. (1989). Chemical and isotopic systematics of oceanic basalts: Implications for mantle composition and processes: *Geological Society of London Special Publication*, 42, 313-345.
- [39] Chappel, B.W. & White, A. J. R. (1974). Two contrasting granite types [abs]. *Pacific Geology*, 8, 173-174.
- [40] Kotková, J. & Harley, S. L. (2010). Anatexis during High-pressure Crustal Metamorphism: Evidence from Garnet-Whole-rock REE Relationships and Zircon-Rutile Ti-Zr Thermometry in Leucogranulites from the Bohemian Massif. *Journal of Petrology*, 51, 1967-2001.
- [41] Gaspar, M., Knaack, C., Meinert, L. & Moretti, D. (2008). REE in skarn systems: A LA-ICP-MS study of garnets from the Crown Jewel gold deposit. *Geochimica Cosmochimica Acta*, 72, 185-205.
- [42] Meinert, L. D. (1989). A review of skarns that contain gold, In D R Lentz Ed., Mineralized intrusion-related skarn systems. *Mineralogical Association of Canada*, Short Course, 26, 359-414.
- [43] Ferry, J. M., Wing, B. A., Penniston-Dorland S.C. & Rumble, D. (2001). The direction of fluid flow during contact metamorphism of siliceous carbonate rocks; new data for the Monzoni and Predazzo aureole, northern Italy, and a global review. *Contribution Mineralogy and petrology*, 142, 679-699.
- [44] Dziggela, A., Wulffa, K., Kolbb, J., Meyera, F. M. & Lahaye, Y. (2009). Significance of oscillatory and bell-shaped growth zoning in hydrothermal garnet: Evidence from the Navachab gold deposit, Namibia. *Chemical Geology*, 262, 262-276.
- [45] Huckenholz, H. G. & Fehr, K. T. (1982). Stability relationships of grossular + quartz + wollastonite + anorthite II. The effect of grandite-hydrograndite solid solution. *Neues Jahrbuch Fur Geology Und Palaontology*, 145, 1-33.
- [46] Hatch, D. M. & Griffen, D. T. (1989). Phase transitions in the grandite garnets. *American Mineralogy*, 74, 151-159.
- [47] Jamtveit, B. (1991). Oscillatory zonation patterns in hydrothermal grossular-andradite garnet: Nonlinear dynamics in regions of immiscibility. *American Mineralogy*, 76, 1319-1327.
- [48] Lentz, D. R. (1998). (ed), Mineralized intrusion-related skarn systems. *Mineralogical Association of Canada*, Short Course, 26, 664.
- [49] Clechenko, C. C. & Valley, J. W. (2003). Oscillatory Zoning in garnet from the Willsboro wollastonite Skarn, Adirondack Mts, New York: a record of shallow hydrothermal processes preserved in a granulite facies terrane. *Journal of Metamorphic Geology*, 21, 771-784.
- [50] Yardley, B. W. D., Rochelle, C. A., Barnicoat, A. C. & Lloyd, G. E. (1991). Oscillatory zoning in metamorphic minerals: an indicator of infiltration metasomatism. *Mineralogical Magazine*, 55, 357-365.
- [51] Meinert, L. D., Dipple, G. & Nicolescu, S. (2005). *World Skarn Deposits*: in Hedenquist J. W., Thompson, J. F. H., Goldfarb R. Richards, J. P, (eds.), Economic Geology One Hundredth Anniversary Volume, Society of Economic Geologists, Littleton, CO., 299-336.
- [52] Einaudi, M. T. & Burt, D. M. (1982). Introduction Terminology, Classification, and Composition of Skarn Deposits. *Economic Geology*, 77, 745-754.